

Synthesis and Electrochemical Properties of Layered $\text{Li}_{0.9}\text{Ni}_{0.45}\text{Ti}_{0.55}\text{O}_2$

Kisuk Kang,[†] Dany Carlier,[†] John Reed,[†] Elena M. Arroyo,[†] Gerbrand Ceder,^{*,†} L. Croguennec,[‡] and C. Delmas[‡]

Department of Materials Science and Engineering, Massachusetts Institute of Technology, 77 Massachusetts Avenue, Cambridge, Massachusetts 02139, and Institut de Chimie de la Matière Condensée de Bordeaux-CNRS and Ecole Nationale Supérieure de Chimie et Physique de Bordeaux, Université Bordeaux I, 87, Av. du Dr. A. Schweitzer, 33608 Pessac Cedex, France

Received June 9, 2003. Revised Manuscript Received August 7, 2003

New $\text{Li}_{0.9}\text{Ni}_{0.45}\text{Ti}_{0.55}\text{O}_2$ positive electrode materials were synthesized by means of ion exchange from $\text{Na}_{0.9}\text{Ni}_{0.45}\text{Ti}_{0.55}\text{O}_2$. Powder X-ray diffraction (XRD) patterns for these materials indicate that they are isostructural with $\alpha\text{-NaFeO}_2$. The degree of cation disordering in the material depends critically on the synthesis conditions. Higher temperatures and longer ion-exchange times induce more cation disordering. Surprisingly, the partially disordered phase shows better capacity retention than the least disordered phase. First-principles calculations indicated the poor capacity retention in the least disordered phase could be attributed to the migration of Ti^{4+} into the Li layer during the electrochemical testing. The Ti^{4+} migration seems to depend sensitively on the $\text{Ni}^{2+}\text{-Ti}^{4+}$ configuration in the transition metal layer. Density of states (DOS) obtained from first-principles calculations indicate that only Ni participates in the electronic conductivity and that the poor conductivity of this material could be another reason for its low specific capacity.

Introduction

We investigate the structure and electrochemical behavior of $\text{Li}_{0.9}\text{Ni}_{0.45}\text{Ti}_{0.55}\text{O}_2$ using a combination of experiments and first-principles calculations. It was recently demonstrated experimentally^{1–3} and theoretically⁴ that, in $\text{LiNi}_{0.5}\text{Mn}_{0.5}\text{O}_2$, Ni can be cycled from +2 to +4 in a reasonable voltage range while Mn^{4+} remains inactive. The restriction of Mn to the +4 state is what gives this material its high stability, as more reduced valence states of Mn are prone to migration.⁵ As a potential analogue to $\text{Li}(\text{Ni}^{2+}, \text{Mn}^{4+})\text{O}_2$, we have investigated $\text{Li}(\text{Ni}^{2+}, \text{Ti}^{4+})\text{O}_2$. This material is expected to be more difficult to synthesize in the layered $R\bar{3}m$ structure as both Ni^{2+} (0.83 Å) and Ti^{4+} (0.745 Å) have a relatively large ionic size, making them prone to mixing into the Li layer.⁶ Indeed, a direct high-temperature synthesis effort of $\text{Li}_x(\text{Ni}_{1-y}\text{Ti}_y)\text{O}_2$ led to disordered rock salt structures for $y \geq 0.4$.⁷

Several investigators have doped small amounts of Ti into LiNiO_2 ^{7–9} in some cases leading to an improved

capacity over undoped LiNiO_2 . In this work, we attempt to synthesize layered $\text{Li}(\text{Ni}, \text{Ti})\text{O}_2$ by ion exchange from the $\text{Na}(\text{Ni}, \text{Ti})\text{O}_2$ precursor. However, the experimental results and first-principles calculations all point toward a material that is rather prone to transition metal cation migration into the Li layer during the electrochemical cycling.

Experimental Section

Preparation of Precursor Samples. The composition, $\text{Na}_{0.9}\text{Ni}_{0.45}\text{Ti}_{0.55}\text{O}_2$, was chosen to prevent the creation of the NiO impurity phase that always appeared in our trials to synthesize $\text{NaNi}_{0.5}\text{Ti}_{0.5}\text{O}_2$. As a starting material for the ion exchange, $\text{Na}_{0.9}\text{Ni}_{0.45}\text{Ti}_{0.55}\text{O}_2$ was prepared by solid-state reaction from Na_2CO_3 (98+%, Aldrich), NiO (99.3%, J.T. Baker), and TiO_2 anatase (99.9+%, Aldrich). The appropriate amounts of these starting materials were wet ball-milled for 1 day. After drying, this mixture was calcined at 750 °C for several hours, ground using a mortar, and pressed into a pellet shape. The pellet was heated at 1000 °C for 14 h in air or Ar (but both the results showed the same XRD pattern). An excess amount of Na_2CO_3 (10 mol %) was added to compensate for the loss due to the volatilization of sodium at high temperature.

Ion Exchange. The obtained Na-containing green powder was wet ball-milled before ion exchange to reduce the particle size. The powder was added to a solution of 5 M LiBr 10 times excess in 120 °C hexanol for 12 or 48 h or boiling (157 °C) hexanol for 12 or 48 h. After ion exchange, the mixture was filtered to recover the powder and rinsed with hexanol, distilled water, and ethanol several times. Finally, the obtained Li-containing light green powder was dried in the air for a day in an oven.

* To whom correspondence should be addressed. E-mail: gceder@mit.edu.

[†] Massachusetts Institute of Technology.

[‡] Université Bordeaux I.

(1) Lu, Z.; MacNeil, D. D.; Dahn, J. R. *Electrochem. Solid State Lett.* **2001**, *4*, A191.

(2) Ammundsen, B.; Paulsen, J. *Adv. Mater.* **2001**, *13*, 943.

(3) Ohzuku, T.; Makimura, Y. *Chem. Lett.* **2001**, 744.

(4) Reed, J.; Ceder, G. *Electrochem. Solid State Lett.* **2002**, *5* (7), A145.

(5) Reed, J.; Ceder, G.; Van der Ven, A. *Electrochem. Solid State Lett.* **2001**, *4* (6), A78.

(6) Wu, E. J.; Tepeesch, P. D.; Ceder, G. *Philos. Mag. B* **1998**, *77* (4), 1039.

(7) Chang, S. H.; Kang, S.; Song, S. W.; Yoon, J.; Choy, J. H. *Solid State Ionics* **1996**, *86–88*, 171.

(8) Croguennec, L.; Suard, E.; Willmann, P.; Delmas, C. *Chem. Mater.* **2002**, *14*, 2149.

(9) Kim, J.; Amine, K. *Electrochem. Commun.* **2001**, *3*, 52.

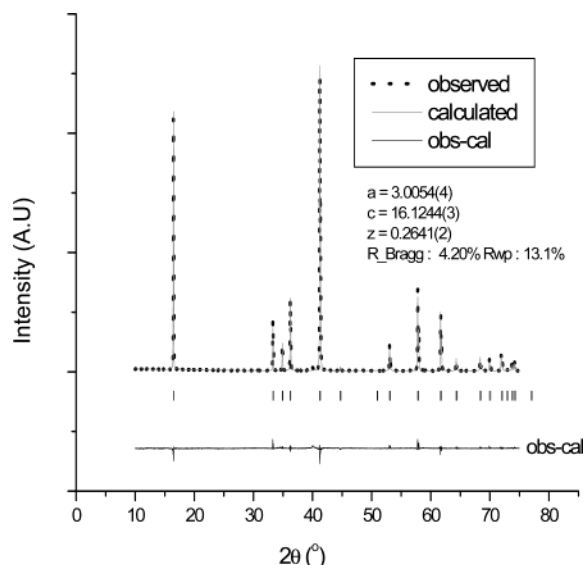


Figure 1. XRD pattern and Rietveld refinement of $\text{Na}_{0.9}\text{Ni}_{0.45}\text{Ti}_{0.55}\text{O}_2$ (a and c are the lattice parameters and z the atomic position of oxygen along the c axis.)

X-ray Diffraction. The XRD pattern was recorded using a Rigaku diffractometer equipped with $\text{Cu K}\alpha$ radiation by step scanning (0.02 or 0.01°/10 s) in the 2θ range of 10–75°. The structure was refined with Fullprof.¹⁰ To prevent a preferred orientation of the material, XRD samples were prepared by spraying the powder to the holder which was pasted with adhesive.

Electrochemical Testing. The lithium cells were configured in the following way: Li/1 M LiPF_6 in EC, DMC = 1:1 (Merck)/ $\text{Li}_{0.9}\text{Ni}_{0.45}\text{Ti}_{0.55}\text{O}_2$ with carbon black (15 wt %) used as a conductive agent and polyethylenetetrafluoride (PTFE) (5 wt %) as binder. Cells were assembled in an argon-filled glovebox and cycled at room temperature using a Maccor 2200 operating in galvanostatic mode. The electrochemical performances of the samples were evaluated upon cycling in the 2.5–4.8 V potential window at C/5, C/10, C/30 and C/50 rate.

Results and Discussion

Structure of $\text{Na}_{0.9}\text{Ni}_{0.45}\text{Ti}_{0.55}\text{O}_2$ and $\text{Li}_{0.9}\text{Ni}_{0.45}\text{Ti}_{0.55}\text{O}_2$. Figure 1 shows the XRD pattern and lattice parameters of $\text{Na}_{0.9}\text{Ni}_{0.45}\text{Ti}_{0.55}\text{O}_2$. Below the measured diffraction pattern are the calculated patterns for the $\alpha\text{-NaFeO}_2$ ($R\bar{3}m$) structure with transition metals (Ni, Ti) in 3b (0,0,0.5) sites, Na in 3a (0,0,0) sites, and O in 6c (0,0, z) sites and the difference between the calculated and observed patterns. Rietveld refinement indicates less than 4% of cation mixing. No additional peaks suggesting ordering between transition metals (Ni and Ti) or between Na and vacancies have been observed. The refined structure parameters are in good agreement with previous studies.^{11,12}

The XRD pattern of the compound $\text{Li}_{0.9}\text{Ni}_{0.45}\text{Ti}_{0.55}\text{O}_2$ shown in Figure 2 is similar to that of LiCoO_2 ($\alpha\text{-NaFeO}_2$ type, space group $R\bar{3}m$) and can be indexed as a hexagonal lattice. This structure has Li ions at the 3a site, the transition metal ions (Ni, Ti) at the 3b site, and O ions at the 6c site. No superlattice peaks from

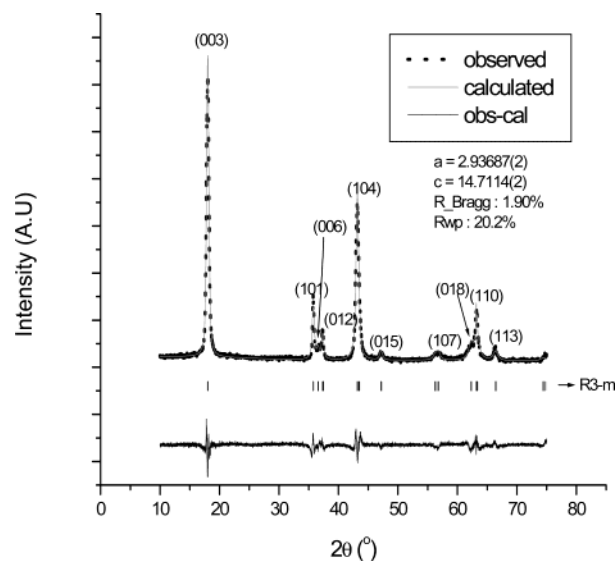


Figure 2. Full pattern matching of $\text{Li}_{0.9}\text{Ni}_{0.45}\text{Ti}_{0.55}\text{O}_2$.

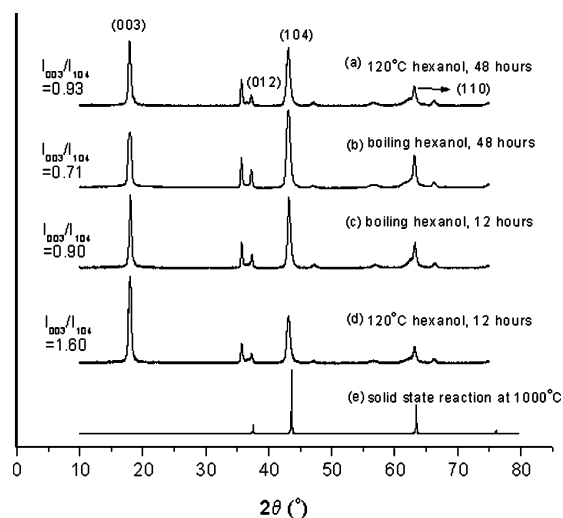


Figure 3. XRD of $\text{Li}_{0.9}\text{Ni}_{0.45}\text{Ti}_{0.55}\text{O}_2$ obtained from different synthesis conditions.

Li-vacancy ordering and Ni–Ti ordering are present in XRD pattern. The structural parameters, obtained from full pattern matching, are in reasonable agreement with the trends obtained by Kim and Amine¹³ for lower Ti contents.⁹ The composition was determined with ICP to be $\text{Li}_{0.79}\text{Na}_{0.12}\text{Ni}_{0.46}\text{Ti}_{0.54}\text{O}_{1.995}$. The total transition metal content was fixed to be unity. Since XRD data indicate that the starting sodium precursor phase is not present anymore after the ion exchange, the residual sodium ions are believed to be present with the lithium ions in the material obtained after the ion exchange. This is indicated by the slightly larger values of a and c lattice parameters than the trends obtained by Kim and Amine.¹³ An accurate Rietveld refinement of site occupancies was not possible due to the relatively broad peaks in the pattern. These are likely caused by an inhomogeneous cation distribution with residual sodium in each particle after the ion exchange. The Na content was independent of ion exchange conditions in the range of times (12–48 h) and temperatures (120–157 °C) tested. However, the relative ratio of the (003) and the (104) peaks systematically decreased as the time and the temperature of the ion exchange process increased. From Figure 3a,b and 3c,d, it can be seen that, for a

(10) Fullprof available at the following URL: <http://www-llb.cea.fr/winplotr/winplotr.htm>.

(11) Nalbandyan, V. B.; Shukaev, I. L. *Russ. J. Inorg. Chem.* **1992**, *37* (11), 1231.

(12) Shin, Y. J.; Yi, M. Y. *Solid State Ionics* **2000**, *132*, 131.

(13) Kim, J.; Amine, K. *J. Power Sources* **2002**, *104*, 33.

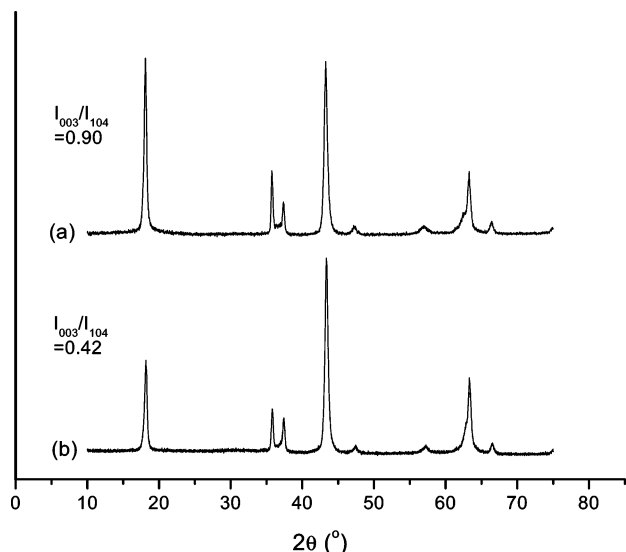


Figure 4. (a) $\text{Li}_{0.9}\text{Ni}_{0.45}\text{Ti}_{0.55}\text{O}_2$ synthesized in boiling hexanol for 12 h (b) after heating in an oven at 160 °C for 2 days.

fixed ion exchange time, an increase in ion exchange temperature leads to a decrease in the ratio of the (003) to (104) peaks. Similarly, a decrease in exchange time leads to an observable increase in the ratio of the (003)/(104) peak intensities at a fixed temperature (e.g., compare pattern 3a,d and 3b,c). It is known that the ratio value of (003)/(104) peak intensities decreases as the degree of cations mixing increases in the layered structure.³ Therefore, our data indicate that longer time and higher temperature ion exchange induces more cation disordering. When we tried to directly synthesize $\text{Li}_{0.9}\text{Ni}_{0.45}\text{Ti}_{0.55}\text{O}_2$ from solid-state reaction, the totally disordered $Fm\bar{3}m$ phase formed (Figure 3e) in agreement with the work by Chang.⁷ This indicates that disordering of cations is favored at elevated temperature.

We obtained further confirmation that prolonged high-temperature exposure leads to more transition metal mixing into the Li layer by taking one of the best layered samples and heating it in air to 160 °C, which caused the 003/104 intensity ratio to decrease further (Figure 4).

From the series of synthesis trials, we believe that the 12-h ion exchange at 120 °C yielded the best layered structure.

First-Principles Calculation of Oxidation States and Voltages. We also investigated the ideal structure with $\text{Ni}/\text{Ti} = 1$, $\text{Li}(\text{Ni}_{0.5}\text{Ti}_{0.5})\text{O}_2$, using first-principles calculations in the spin-polarized generalized gradient approximation to density functional theory. Further computational details are not given in this paper, as they are similar to previous work⁴ on related materials. Calculations on periodic supercells require one to adopt an ordered configuration for the Ni and Ti ions. The smallest supercell has two formula units and can have Ni and Ti ordered in either rows along one of the hexagonal axis or zigzag configurations. We tested both, but found no significant difference between them for the results reported here (voltage, oxidation states, and electronic structure). To determine the oxidation states, the electron spin is integrated around Ni and Ti. The result in Figure 5a gives no unpaired electrons for Ti and about 1.5 spin for Ni, corresponding to Ti^{4+} and Ni^{2+} (approximately). Partial delithiation (Figure 5b) clearly leads to a decrease in spin density of Ni, indicating that Ni^{2+} is oxidized to Ni^{3+} . Further Li removal was found to lead to Ni^{4+} . This result is similar to the $\text{LiNi}_{0.5}\text{Mn}_{0.5}\text{O}_2$ system where the redox couple is $\text{Ni}^{2+}/\text{Ni}^{4+}$ while Mn acts only as a structure stabilizer.⁴ On the basis of the $\text{Ni}^{2+}/\text{Ni}^{4+}$ redox couple, the theoretical capacity is 290.6 mA·h/g. The calculated average voltage between $\text{LiNi}_{0.5}\text{Ti}_{0.5}\text{O}_2$ and $\text{Li}_{0.5}\text{Ni}_{0.5}\text{Ti}_{0.5}\text{O}_2$ is 3.58 V and the voltage between $\text{Li}_{0.5}\text{Ni}_{0.5}\text{Ti}_{0.5}\text{O}_2$ and $\text{Ni}_{0.5}\text{Ti}_{0.5}\text{O}_2$ is 3.84 V. Given that GGA calculations have been found to underestimate the voltage of the $\text{Ni}^{2+}/\text{Ni}^{4+}$ redox couple by about 0.7 V, the charging voltage for $\text{LiNi}_{0.5}\text{Ti}_{0.5}\text{O}_2$ may actually be quite high.⁴

Electrochemistry. The electrochemical properties of three samples with different degrees of cation disordering were evaluated (Figure 6). The first charging capacities were about 110–150 mA·h/g and the first discharge capacities were about 45–95 mA·h/g at a C/50 rate, indicating a significant capacity loss in the first cycle. Assuming that the electrochemical redox couple is $\text{Ni}^{2+}/\text{Ni}^{4+}$ in this material, the first charging capacity is far less than the theoretical capacity (265.1 mA·h/g for $\text{Li}_{0.9}\text{Ni}_{0.45}\text{Ti}_{0.55}\text{O}_2$).

The origin of the low capacity and significant capacity loss at the first cycle could lie in several factors. The poor capacity might be explained by the low electronic conductivity of this material. Several indirect attempts

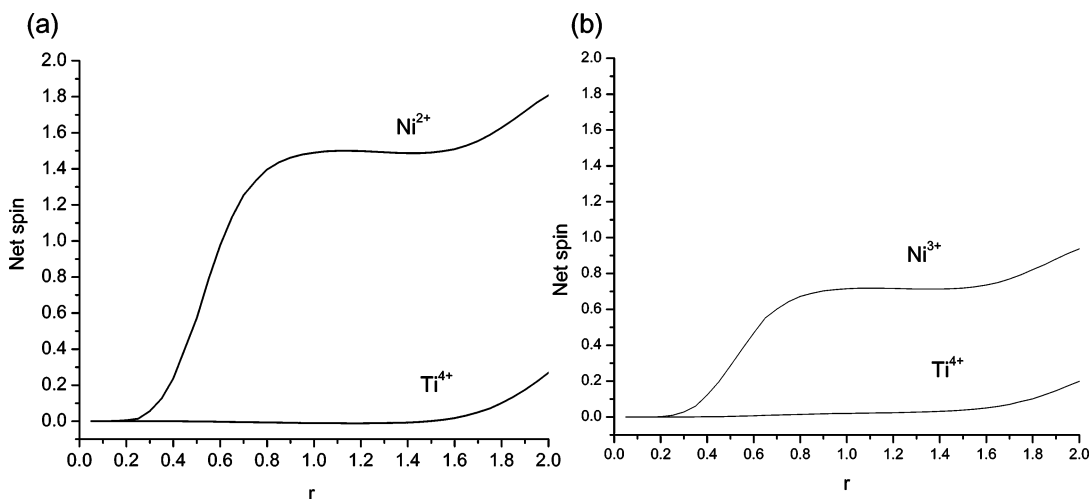


Figure 5. Integrated spin as a function of integration radius (Å) around Ni and Ti in (a) $\text{LiNi}_{0.5}\text{Ti}_{0.5}\text{O}_2$ and (b) $\text{Li}_{0.5}\text{Ni}_{0.5}\text{Ti}_{0.5}\text{O}_2$.

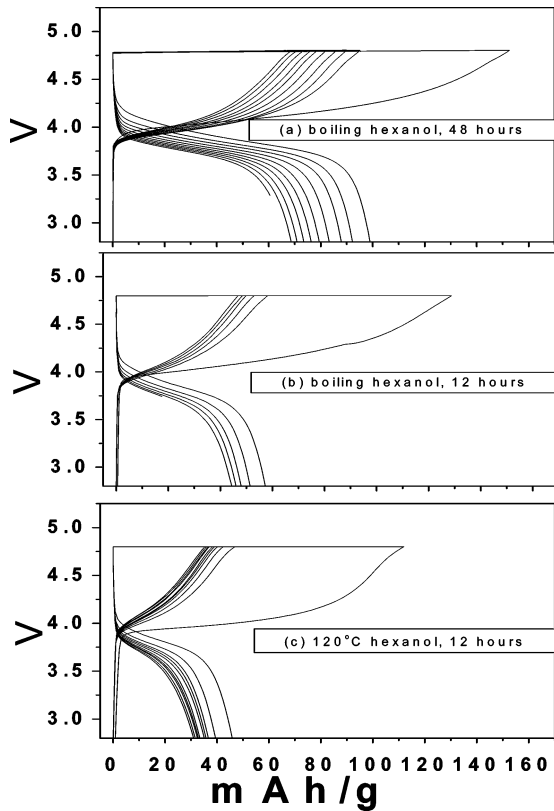


Figure 6. Galvanostatic cycling of $\text{Li}_{0.9}\text{Ni}_{0.45}\text{Ti}_{0.55}\text{O}_2$ samples.

were made to evaluate the conductivity. One of them was to deduce information on conductivity from the calculated density of states of the lithiated and the partially delithiated states of this material. While band gaps are notoriously unreliable in LDA or GGA, some information on conductivity can be deduced from the nature of the occupied and lowest unoccupied states. Figure 7 shows the electronic density of states for $\text{LiNi}_{0.5}\text{Ti}_{0.5}\text{O}_2$ and $\text{Li}_{0.5}\text{Ni}_{0.5}\text{Ti}_{0.5}\text{O}_2$. In $\text{LiNi}_{0.5}\text{Ti}_{0.5}\text{O}_2$, the Fermi level resides in a gap between the filled majority spin Ni e_g states and the unfilled minority spin Ni e_g . In $\text{Li}_{0.5}\text{Ni}_{0.5}\text{Ti}_{0.5}\text{O}_2$, the Fermi level is in the pseudo-gap between Ni e_g states. Clearly, at both Li compositions, the Ti states are rather far removed from the Fermi level, and it is, therefore, likely that only Ni participates in the electronic conductivity in this material. Given that Ni occupies less than 50% of the transition metal

layer positions and is randomly distributed, the Ti-rich region can act to reduce electronic transport. We could not perform a direct electronic conductivity measurement on the samples as sintering them leads to irreversible structural changes.

We also compared the specific capacities at different C rates. As shown in Figure 8, the capacity reduces dramatically with increasing C-rate, consistent with some transport limitation in the material. Moreover, the large potential drop after the first charging indicates that there is a large resistance in the cell, which we attribute to the large resistance of the positive electrode.

Surprisingly, the samples that are believed to be the most layered suffer the largest first-cycle capacity loss. While in situ or post-cycling ex situ XRD studies are required to clarify the structural changes associated with the capacity loss, we speculate that it may be related to Ti^{4+} migration into the Li layer, as has been observed for Na_xTiO_2 .¹⁴ Since Ti^{4+} has no d electrons, ligand-field effects do not contribute to any octahedral stabilization energy. This may make Ti migration into the Li layer, which requires passing through tetrahedral sites, easier.⁵ Using first-principles calculations, we attempted to determine the activation barrier for Ti^{4+} migration into the Li layer. For a transition metal ion to migrate into the Li layer, it needs to successively pass through an oxygen triangle connecting the octahedral site in the transition metal layer, a tetrahedral site, and another oxygen triangle connecting it to the octahedral site in the Li layer. This migration path is complex with typically two maxima as the ion passes through the faces between the octahedral and tetrahedral and a local minimum in the tetrahedral and octahedral sites. A Li trivacancy was always present in the calculations, as transition metals will not move into the tetrahedral site unless the three Li sites that share faces with it are vacant. Such trivacancies occur frequently at high states of charge. The result revealed a complicated dependence of Ti^{4+} stability on its local environment. Overall, Ti^{4+} migration was easiest when surrounded by other Ti^{4+} . In $\text{Li}_{0.5}\text{TiO}_2$, a tetrahedral Ti defect actually lowers the energy by about 0.15 eV. As Ti becomes surrounded by more Ni^{2+} , we found that migration of Ti into the tetrahedral site becomes unfavorable due to the strong electrostatic effective attraction between Ti^{4+} and Ni^{2+} in the transition metal layer. A Ti^{4+} surrounded by only

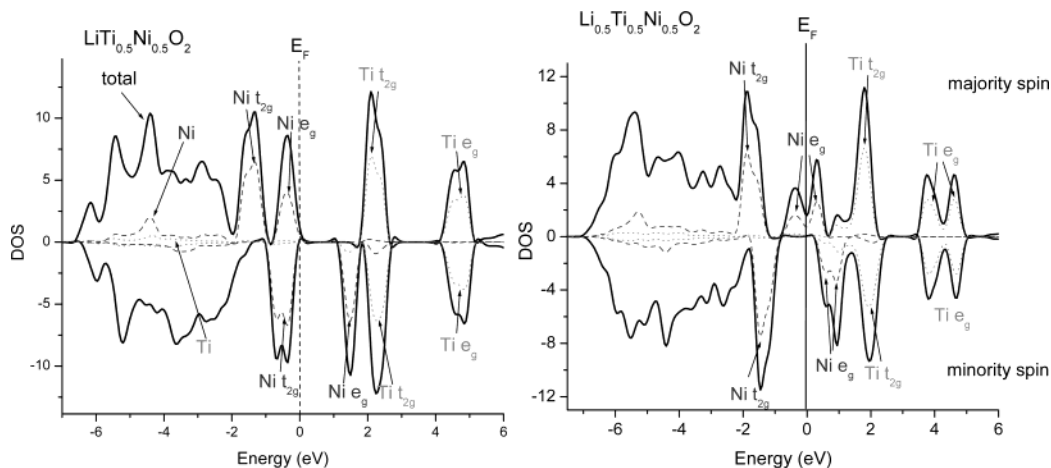


Figure 7. Spin density of state of the 3d orbitals of Ni and Ti in $\text{LiNi}_{0.5}\text{Ti}_{0.5}\text{O}_2$ and $\text{Li}_{0.5}\text{Ni}_{0.5}\text{Ti}_{0.5}\text{O}_2$.

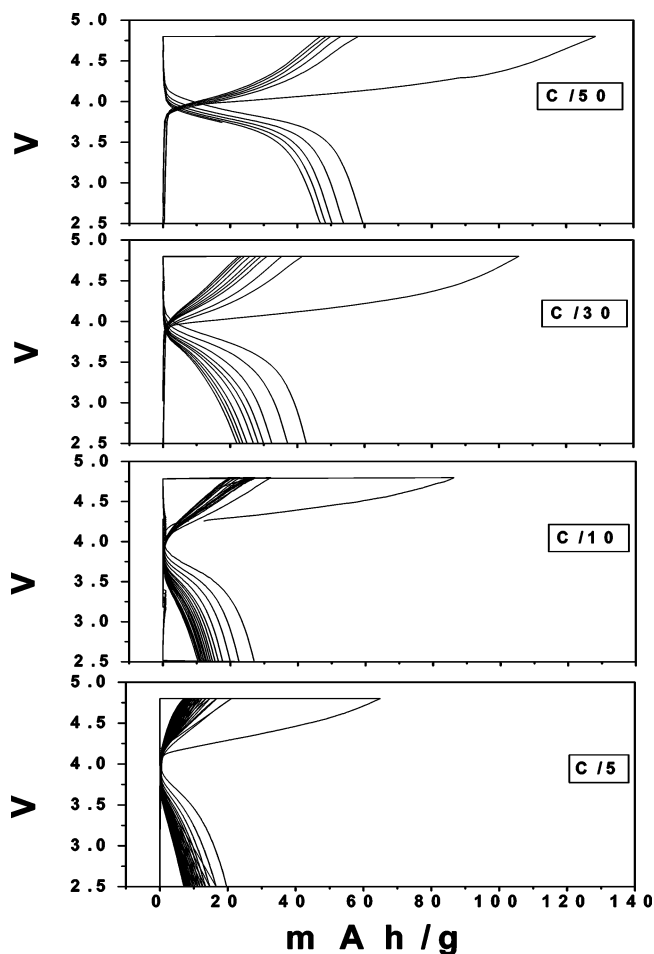


Figure 8. Galvanostatic cycling of $\text{Li}_{0.9}\text{Ni}_{0.45}\text{Ti}_{0.55}\text{O}_2$ sample (boiling hexanol, 12 h) at a different C rate.

Ni^{2+} requires about 0.45 eV to go into the tetrahedral site. This may explain why small amounts of Ti doping in LiNiO_2 result in a very stable material with little capacity fade.⁹

(14) Maazaz, A.; Delmas, C.; Hagemuller, P. *J. Inclusion Phenom.* **1983**, *1*, 45.

Given the high concentration of Ti^{4+} in our sample, Ti^{4+} migration into the Li layer seems likely for the well-ordered samples (Figure 6c,b). If the sample already has immobile transition metal ions in the layer, the probability that trivacancies occur in the Li layer during charging is significantly reduced. As a result, less Ti^{4+} migration is expected during cycling. This may explain why the more disordered sample actually has smaller first-cycle capacity loss.

Conclusions

We have successfully synthesized layered $\text{Li}_{0.9}\text{Ni}_{0.45}\text{Ti}_{0.55}\text{O}_2$ through ion exchange from $\text{Na}_{0.9}\text{Ni}_{0.45}\text{Ti}_{0.55}\text{O}_2$. The material has a significant tendency for transition metal cation mixing into the Li layer, as evidenced by the disordered product obtained in direct high-temperature synthesis of the Li compound. This disordering also limits the time and temperature of the ion exchange process and may be the root cause of the significant first-cycle capacity loss. On the basis of the results of first-principles calculations, we speculate this capacity loss to be due to Ti^{4+} migration into the Li layer, though further structural characterization is required to demonstrate this conclusively.

Acknowledgment. The authors would like to thank Prof. Clare Grey and Dr. Wonsub Yoon for the fruitful discussion. This work was supported by the Assistant Secretary for Energy Efficiency and Renewable Energy, Office of FreedomCAR and Vehicle Technologies of the U.S. Department of Energy under Contract No. DE-AC03-76SF00098, Subcontract No. 6517748 with the Lawrence Berkeley National Laboratory, and by the US–France cooperative agreement NSF-INT-0003799. The authors are grateful to Prof. Bing Joe Hwang, Dr. Dane Morgan, Dr. Eric Wu, and Dr. Anton Van der Ven for the valuable advice.

CM034455+